ELSEVIER

Journal of Alloys and Compounds 452 (2008) 110–115

Journal of ALLOYS AND COMPOUNDS

www.elsevier.com/locate/jallcom

Thermodynamic study of LiF–BeF_2–ZrF_4–UF_4 system

O. Beneš *, R.J.M. Konings

European Commission, Joint Research Centre, Institute for Transuranium Elements, P.O. Box 2340, 76125 Karlsruhe, Germany

Received 18 September 2006; received in revised form 5 January 2007; accepted 22 January 2007
Available online 12 March 2007

Abstract

In this work the three binary phase diagrams LiF–ZrF_4, BeF_2–ZrF_4 and UF_4–ZrF_4 were thermodynamically assessed. The three ternary phase diagrams LiF–BeF_2–ZrF_4, BeF_2–ZrF_4–UF_4 and LiF–ZrF_4–UF_4 were approximated on the basis of binary data. A pseudo-ternary LiF–BeF_2–ZrF_4 system with constant amount of UF_4 set to 0.83 mol% was calculated as well, typical for molten salt reactor fuel. Based on this diagram a suggestion for the composition of the fuel in this system was made.

Keywords: Nuclear fuel; Phase diagram; Molten fluoride salt; Thermodynamics

1. Introduction

The molten salt reactor (MSR) belongs to the Generation IV reactor concepts. It is based on the dissolution of the fissile material (^{233}U, ^{235}U, ^{239}Pu) in an inorganic fluid which circulates from the reactor core to the heat exchanger and back. A big advantage of this concept is its possibility to perform on-site clean up of the fuel from the fission products, that would normally slow down the chain reaction by capturing the neutrons. This clean up can be done either on-line or in batch process and the processed salt is returned into the cycle. Other advantages of this concept are the relatively low inventory of the fissile material, high fuel burn-up, possibility of the actinide waste burning and efficient power production. Because the operating temperatures of this reactor can exceed 800 °C it can be also used for hydrogen production. A very important property of this system is its safety. Firstly the whole circuit is kept under the atmospheric pressure (boiling temperature is around 1400 °C) avoiding the major driving force, the high pressure, of the radioactivity release during accidents. Secondly this system has a very high negative void coefficient, which means that with increasing temperature the chain reaction is slowed down. This is based on the fact that when the molten salt is heated it expands and pushes the fissile material out of the reactor core. The first concept of the molten salt reactor was made in the 1950s and was known as the US Aircraft Reactor Experiment (ARE). In 1960s the Oak Ridge National Laboratory (ORNL) took the lead in this field of research and in the next decade their effort culminated in the construction and operation of the Molten Salt Reactor Experiment (MSRE). This MSRE was a graphite moderated test reactor located in ORNL with the output of 7.4 MW. In the 1970s the molten salt breeder reactor (MSBR) concept was introduced. It was a prototype breeder reactor with the output of 2250 MW_{th} that produced more fissile material than it consumed. But this project was abandoned and the attention was shifted to other designs, principally the sodium-cooled fast breeder. Nowadays the MSR project is in the scope of the renewed interest. As a fuel the molten fluoride salts were chosen, because their properties fulfill most of the following requirements [1]:

- Thermodynamic stability at high temperatures;
- Low neutron capture cross-section;
- Stability to radiation (no radiolytic decomposition);
- Low vapor pressure above the liquid surface at operating temperatures;
- Low melting point;
- Good solubility for uranium, plutonium and thorium.

One of the disadvantages of the fluoride salt is its chemical aggressivity to the construction material, but the nickel-based alloys (Hastelloy) are very resistant and can be used for the structural components.

* Corresponding author. Tel.: +49 7247 951263; fax: +49 7247 951566.
E-mail address: ondrej.benes@cec.eu.int (O. Beneš).

0925-8388/$ – see front matter © 2007 Elsevier B.V. All rights reserved.
doi:10.1016/j.jallcom.2007.01.184

In this work we present the thermodynamic description of the $LiF–BeF_2–ZrF_4–UF_4$ quaternary system, a system that has been used in the MSRE. The comparison between our modelled values and the values made by ORNL in the 1960s is made as well. In this system the LiF and BeF_2 compounds serve as a matrix for dissolving the fissile uranium in the form of UF_4, while the ZrF_4 compound is added in small concentrations (around 5%) as an oxygen getter.

For the reactor design it is very important to have the thermodynamic description, because it is impossible to measure every composition of the solution. Once the system is thermodynamically described it is easier to optimize the fuel choice and to predict its properties.

2. Thermodynamic modeling

To describe a T–X phase diagram the Gibbs energy equations of all compounds and the Gibbs equations of mixing, in case a solution is created, are required. If these data are not known they need to be obtained by thermodynamic assessment. This was all done according to the CALPHAD method, including the critical review of all available data of interest, followed by the optimization of unknown data to get the best possible fit between calculated values and experimental data. Because the data for ternary systems are usually not known, first the binary phase diagrams need to be evaluated and then the higher order systems can be extrapolated according to the Kohler–Toop formalism [2]. All optimizations were performed using the OptiSage module in FactSage 5.4 software [3], which uses the Bayesian optimization algorithm [4]. This algorithm is based on the estimation of a probability distribution function.

2.1. Condensed phases

The Gibbs energy equation for relevant compounds is described by Eq. (1) as a contribution of the enthalpy of formation, absolute entropy at reference state and heat capacity.

$$G(T) = \Delta_f H^\circ(298.15\,\mathrm{K}) - S^\circ(298.15\,\mathrm{K})T + \int_{298.15}^{T} C_p(T)\,\mathrm{d}T - T\int_{298.15}^{T}\left(\frac{C_p(T)}{T}\right)\mathrm{d}T \quad (1)$$

There are 13 condensed phases in the studied $LiF–BeF_2–ZrF_4–UF_4$ system. These are four endmembers, eight binary intermediate phases and one ternary intermediate compound. The thermodynamic data for LiF, BeF_2, ZrF_4, UF_4 are known and were taken from an internal report [5] and the data for intermediate compounds Li_2BeF_4, Li_4UF_8, LiU_4F_{17} and $LiUF_5$ were taken from Ref. [6]. Data for Li_2ZrF_6, Li_3ZrF_7, Li_4ZrF_8, $Li_3Zr_4F_{19}$ and Li_6BeZrF_{12} are not known and had to be assessed. All thermodynamic data for condensed phases concerned in our work are summarized in Table 1.

2.2. Excess parameters for binary solutions

All the solutions concerned in this work were treated as non-ideal. The general formula for such a solution is defined by Eq. (2) as the weighted average of the Gibbs energies of the pure components plus the contribution of ideal mixing and the excess Gibbs energy:

$$G(T) = x_1G_1(T) + x_2G_2(T) + x_1RT\,\ln x_1 + x_2RT\,\ln x_2 + {}_{xs}G \quad (2)$$

Table 1
Gibbs energy functions for the pure components and intermediate compounds of the system $LiF–BeF_2–ZrF_4–UF_4$; $G(T) = A + BT + C\,T\,\ln T + DT^2 + ET^{-1} + FT^3$

Compound	$A \times 10^{-6}$	$B \times 10^{-2}$	C	D	E	F
LiF(l)[a]	−0.617790	3.86910	−6.4183E+01			
BeF_2(l)[a]	−1.035874	2.27400	−4.0984E+01	−2.2468E−02		
ZrF_4(l)[a]	−1.881201	6.708110	−1.2360E+02			
UF_4(l)[a]	−1.966757	10.5494	−1.7474E+02			
LiF(cr)[a]	−0.632482	2.62493	−4.3309E+01	−8.1561E−03	−2.84562E+05	−8.4117E−08
BeF_2(cr, α)[a,b]	−1.037387	1.07771	−1.9181E+01	−5.4769E−02		
BeF_2(cr, β)[a,b]	−1.039380	2.21961	−3.9457E+01	−2.3128E−02		
ZrF_4(cr)[a]	−1.952049	6.84744	−1.1561E+02	−1.0250E−02	8.00255E+05	
UF_4(cr)[a]	−1.950643	6.23757	−1.1452E+02	−1.0277E−02	−2.06580E+05	
Li_2BeF_4(cr)[a]	−2.307288	5.21881	−9.0779E+01	−7.4575E−02	−9.85416E+04	3.0693E−09
Li_4UF_8(cr)[c]	−4.460463	16.1734	−2.8672E+02	−4.4921E−02	−1.34364E+06	
$LiUF_5$(cr)[c]	−2.605258	8.90824	−1.5757E+02	−1.8938E−02	−4.90845E+05	
LiU_4F_{17}(cr)[c]	−8.528884	28.2132	−5.0113E+02	−4.9771E−02	−1.11058E+06	
Li_4ZrF_8(cr)[d]	−4.501968	17.0946	−2.8885E+02	−4.2875E−02	−1.93850E+06	−3.3647E−07
Li_3ZrF_7(cr)[d]	−3.803428	13.6026	−2.4554E+02	−3.4718E−02	−1.65394E+06	−2.5235E−07
Li_2ZrF_6(cr)[d]	−3.222317	11.6681	−2.0223E+02	−2.6562E−02	−1.36938E+06	−1.6823E−07
$Li_3Zr_4F_{19}$(cr)[d]	−9.645139	33.66443	−5.9238E+02	−6.5470E−02	−4.05470E+06	−2.5235E−07
Li_6BeZrF_{12}(cr)[d]	−6.823700	23.4100	−3.9310E+02	−1.1700E−02	−9.05300E+05	

[a] Data taken from an internal report [5].
[b] A transition from α-form to β-form occurs at 500 K.
[c] Taken from Ref. [6].
[d] Obtained by the assessment with general polynomial model.

Table 2
Excess Gibbs energy coefficients for the binary solutions—according to Eq. (3)

Interaction	i	j	A	B
$LiF–ZrF_4$[a]	1	1	6,236	1.33
	2	1	−102,338	−3.29
	1	2	−84,015	1.10
$BeF_2–ZrF_4$[a]	1	1	−7,143	18.02
	1	2	−43,839	5.93
$UF_4–ZrF_4$[a]	1	1	−20,150	0
	1	2	−48,350	0
	1	3	−127,500	0
$UF_4–ZrF_4$[b]	1	1	−33,200	0
	1	2	−20,000	0
	1	3	−65,000	0

[a] Liquid solution.
[b] Solid solution.

For the description of the excess Gibbs energy the classical polynomial model was used. The general formula for such a model is shown in Eq. (3), where the A and B terms are the parameters to be optimized, x_1, x_2 are the molar ratios of the components that the solution consists of, and i, j are their power coefficients, respectively:

$$_{xs}G = \sum_{i,j} x_1^i x_2^j (A + BT) \quad (3)$$

$LiF–ZrF_4$, $BeF_2–ZrF_4$ and $ZrF_4–UF_4$ binary systems were assessed in this work. The values for excess Gibbs functions are shown in Table 2. Assuming these data together with the data from previous work [6] the quaternary $LiF–BeF_2–ZrF_4–UF_4$ system has been modelled.

2.3. Ternary assessments

After the binary phase diagrams had been evaluated the higher order systems were extrapolated according to the Kohler–Toop asymmetric formalism [2]. In case of the $BeF_2–ZrF_4–UF_4$ system the asymmetric compound was BeF_2, since the UF_4 and ZrF_4 have very similar physical properties. For the $LiF–BeF_2–ZrF_4$ and $LiF–ZrF_4–UF_4$ systems LiF was chosen to be asymmetric, because it most likely creates ionic species in the liquid compared to the other components that form molecular species. Small ternary interactions were considered only in the $LiF–BeF_2–ZrF_4$ system, i.e.,

$$_{xs}G_{ternary} = x_1 x_2 x_3 (-6523) \quad (4)$$

The $LiF–BeF_2–UF_4$ ternary system was calculated in the previous work [6].

3. Results and discussion

3.1. Binary subsystems

Six binary subsystems are concerned in the $LiF–BeF_2–ZrF_4–UF_4$ system. The $LiF–BeF_2$, $LiF–UF_4$ and $BeF_2–UF_4$ were assessed by van der Meer et al. [6]. The assessment of $LiF–ZrF_4$ system was based on the experimental data from Thoma at al. [7,8]. It consists of four intermediate phases, three eutectics and one peritectic, where the $Li_3Zr_4F_{19}$ decomposes. Our modelled values for eutectics are: $E_1 = 882\,K$ at $X_{ZrF_4} = 0.192$, $E_2 = 855\,K$ at $X_{ZrF_4} = 0.325$ and $E_3 = 775\,K$ at $X_{ZrF_4} = 0.473$, while the peritectic correspond to $P = 798\,K$ at $X_{ZrF_4} = 0.51$. All the values are in excellent agreement with the experimental data. The Li_3ZrF_7 and Li_2ZrF_6 compounds melt congruently at $T = 934\,K$ and 856 K, respectively, while the last intermediate compound Li_4ZrF_8 decomposes at $T = 762\,K$. The assessed phase diagram of $LiF–ZrF_4$ system is shown in Fig. 1.

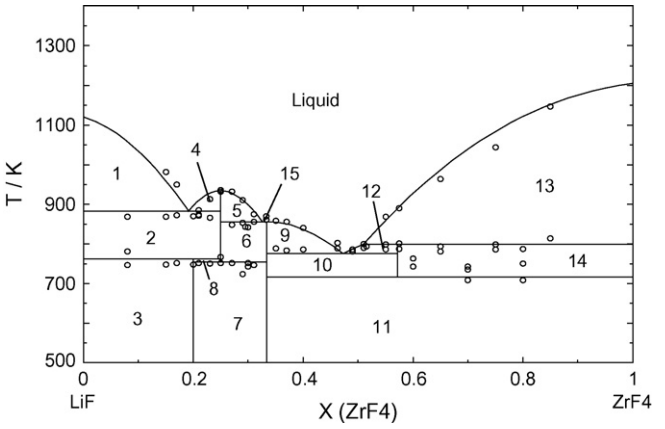

Fig. 1. The calculated diagram of the $LiF–ZrF_4$ system. (◯) Results by Thoma et al. [7]. Phase fields: (1) LiF + L; (2) LiF + Li_3ZrF_7; (3) LiF + Li_4ZrF_8; (4) Li_3ZrF_7 + L; (5) Li_3ZrF_7 + L; (6) Li_3ZrF_7 + Li_2ZrF_6; (7) Li_4ZrF_8 + Li_2ZrF_6; (8) Li_4ZrF_8 + Li_3ZrF_7; (9) Li_2ZrF_6 + L; (10) Li_2ZrF_6 + $Li_3Zr_4F_{19}$; (11) Li_2ZrF_6 + ZrF_4; (12) $Li_3Zr_4F_{19}$ + L; (13) ZrF_4 + L; (14) $Li_3Zr_4F_{19}$ + ZrF_4; (15) Li_2ZrF_6 + L; L: liquid.

The $BeF_2–ZrF_4$ system optimization was based on the data by Thoma et al. [8] and the resulting phase diagram is shown in Fig. 2. It is a single eutectic system ($T = 806\,K$ at $X_{ZrF_4} = 0.016$) with the region of immiscibility starting at the monotectic temperature of 913 K with the critical temperature of 1015 K. The shape of the liquidus line in the ZrF_4-rich side in our work differs from the one proposed by Thoma et al. However their interpretation of the experimental data is not in agreement with thermodynamic rules (the first derivative of the liquidus curve

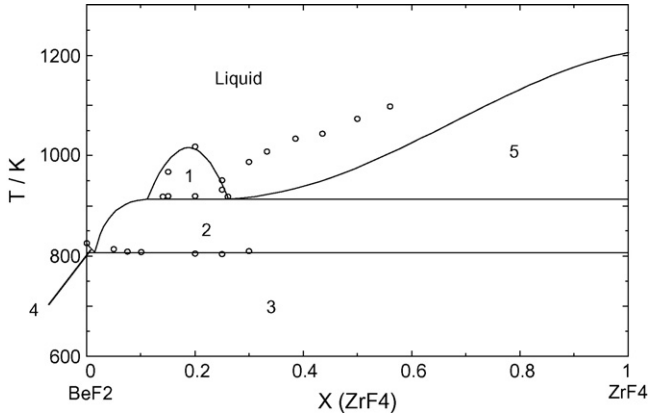

Fig. 2. The calculated diagram of the $BeF_2–ZrF_4$ system. (◯) Results by Thoma et al. [8]. Phase fields: (1) $L_1 + L_2$; (2) ZrF_4 + L; (3) ZrF_4 + $BeF_2(\beta)$; (4) $BeF_2(\beta)$ + L; (5) ZrF_4 + L; L: liquid.

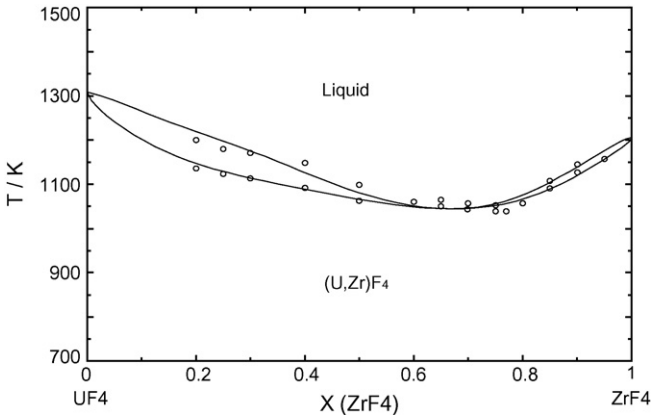

Fig. 3. The calculated diagram of the UF_4–ZrF_4 system. (◯) Results by Barton et al. [9].

must be zero at the border of the miscibility gap). At the same time our model has very good agreement with the experimental data at the BeF_2-rich side. An alternative would be to model whole diagram as a single eutectic system without the miscibility gap like BeF_2–UF_4 and BeF_2–ThF_4 with probably the best absolute agreement. Nevertheless this idea was rejected because of the observation of the miscibility gap by quenching experiments [8]. For the future it might be interesting to make some new experiments in this system. Since the vapor pressure of ZrF_4 is rather high these must be performed in gas tight crucibles.

The UF_4–ZrF_4 system is the simplest one consisting of the solid solution in whole range with the eutectic point at $T = 1043$ K and $X_{ZrF_4} = 0.67$. The diagram is shown in Fig. 3 and is in quite good agreement with the experimental data of Barton et al. [9].

It is well known that the activity of gaseous phase of ZrF_4 becomes equal to 1 at a temperature lower than its melting point, but for the construction of Figs. 1–3 the gas phase was suppressed, yielding the meta-stable solid–liquid equilibrium.

3.2. Ternary subsystems

Using the data from the binary subsystems the four ternary diagrams were extrapolated: LiF–BeF_2–UF_4, LiF–BeF_2–ZrF_4, LiF–ZrF_4–UF_4 and BeF_2–ZrF_4–UF_4. The ternary subsystem LiF–BeF_2–UF_4 was described in Ref. [6], while the other three are calculated in this work.

The LiF–BeF_2–ZrF_4 system, shown in Fig. 4 has seven invariant points; three eutectics and four peritectics. The lowest eutectic calculated at $T = 660$ K and $X_{LiF} = 0.475$, $X_{BeF_2} = 0.490$, $X_{ZrF_4} = 0.035$ is in reasonable agreement with the data of Thoma et al. [8] who reported $T = 628$ K and $X_{LiF} = 0.48$, $X_{BeF_2} = 0.50$, $X_{ZrF_4} = 0.02$. The other invariant points, its coordinates and the solid phases presented in equilibrium are shown in Table 3. A big miscibility gap appears in the BeF_2-rich region, which was also found experimentally by Thoma et al. A pseudo-ternary section at $X_{ZrF_4} = 0.16$ was calculated for the better understanding of the system and is shown in Fig. 5. Since a significant amount of experimental work was done on this ternary system [8], the comparison between the liquidus points

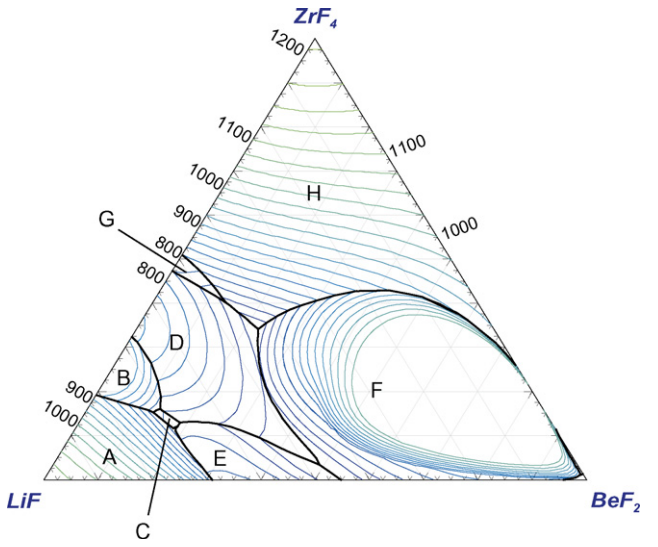

Fig. 4. Liquidus projection of the LiF–BeF_2–ZrF_4 ternary system. Primary phase fields: (A) LiF; (B) Li_3ZrF_7; (C) Li_4ZrF_8; (D) Li_2ZrF_6; (E) Li_2BeF_4; (F) $BeF_2(\beta)$; (G) $Li_3Zr_4F_{19}$; (H) ZrF_4.

and our calculated data was performed. The result is shown in Fig. 6 as a function of temperature and a good agreement is evident. As it can be seen all the data are within ±10%, while 69% of the data agree better than ±5%.

The LiF–ZrF_4–UF_4 system contains eight invariant points; three eutectics and five peritectics. All invariant points, its coordinates and the solid phases present in equilibrium are listed in Table 3. The phase diagram is shown in Fig. 7. The phase diagram of BeF_2–ZrF_4–UF_4 system is shown in Fig. 8 and is characterized by a huge miscibility gap. No invariant points are found in this system.

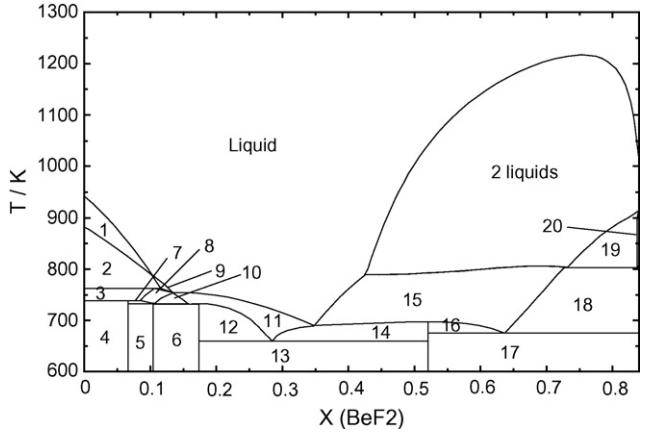

Fig. 5. Pseudo-binary section through the LiF–BeF_2–ZrF_4 phase diagram at $X_{ZrF_4} = 0.16$. Phases: (1) LiF + L; (2) LiF + Li_3ZrF_7 + L; (3) LiF + Li_4ZrF_8 + L; (4) LiF + Li_4ZrF_8 + Li_6BeZrF_{12}; (5) Li_4ZrF_8 + Li_2ZrF_6 + Li_6BeZrF_{12}; (6) Li_2ZrF_6 + Li_2BeF_4 + Li_6BeZrF_{12}; (7) Li_4ZrF_8 + Li_6BeZrF_{12} + L; (8) Li_4ZrF_8 + L; (9) Li_3ZrF_7 + L; (10) Li_4ZrF_8 + Li_2ZrF_6 + L; (11) Li_2ZrF_6 + L; (12) Li_2ZrF_6 + Li_2BeF_4 + L; (13) Li_2ZrF_6 + Li_2BeF_4 + $BeF_2(\beta)$; (14) Li_2ZrF_6 + $BeF_2(\beta)$ + L; (15) $BeF_2(\beta)$ + L; (16) Li_2ZrF_6 + $BeF_2(\beta)$ + L; (17) Li_2ZrF_6 + (U,Zr)F_4 + $BeF_2(\beta)$; (18) (U,Zr)F_4 + $BeF_2(\beta)$ + L; (19) (U,Zr)F_4 + L_1 + L_2; (20) (U,Zr)F_4 + L; L, liquid.

Table 3
Calculated invariant points in the LiF–BeF_2–ZrF_4 and LiF–ZrF_4–UF_4 systems

System	X_{LiF}	X_{BeF_2}	X_{ZrF_4}	X_{UF_4}	T (K)	Equilibrium	Solid phase present
LiF–BeF_2–ZrF_4	0.475	0.490	0.035	0	660	Eutectic	$Li_2ZrF_6 + LiBe_2F_4 + BeF_2(\beta)$
	0.434	0.224	0.342	0	676	Eutectic	$ZrF_4 + Li_2ZrF_6 + BeF_2(\beta)$
	0.684	0.186	0.130	0	731	Eutectic	$Li_2ZrF_6 + LiBe_2F_4 + Li_6BeZrF_{12}$
	0.706	0.134	0.160	0	754	Peritectic	$Li_3ZrF_7 + Li_4ZrF_8 + Li_2ZrF_6$
	0.696	0.184	0.119	0	737	Peritectic	$Li_2BeF_4 + Li_6BeZrF_{12} + Li_4ZrF_8$
	0.463	0.136	0.401	0	714	Peritectic	$Li_2ZrF_6 + ZrF_4 + Li_3Zr_4F_{19}$
	0.721	0.126	0.153	0	760	Peritectic	$Li_4ZrF_8 + LiF + Li_3ZrF_7$
LiF–ZrF_4–UF_4	0.578	0	0.262	0.160	666	Eutectic	$LiUF_5 + Li_2ZrF_6 + (U,Zr)F_4$
	0.639	0	0.213	0.148	668	Eutectic	$LiUF_5 + Li_4ZrF_8 + Li_2ZrF_6$
	0.512	0	0.475	0.014	770	Eutectic	$Li_3Zr_4F_{19} + Li_2ZrF_6 + (U,Zr)F_4$
	0.674	0	0.172	0.154	681	Peritectic	$LiUF_5 + Li_4ZrF_8 + LiF$
	0.720	0	0.035	0.245	744	Peritectic	$LiUF_5 + LiF + Li_4UF_8$
	0.540	0	0.262	0.199	727	Peritectic	$LiUF_5 + (U,Zr)F_4 + LiU_4F_{19}$
	0.717	0	0.217	0.065	760	Peritectic	$Li_4ZrF_8 + LiF + Li_3ZrF_7$
	0.701	0	0.230	0.069	754	Peritectic	$Li_4ZrF_8 + Li_2ZrF_6 + Li_3ZrF_7$

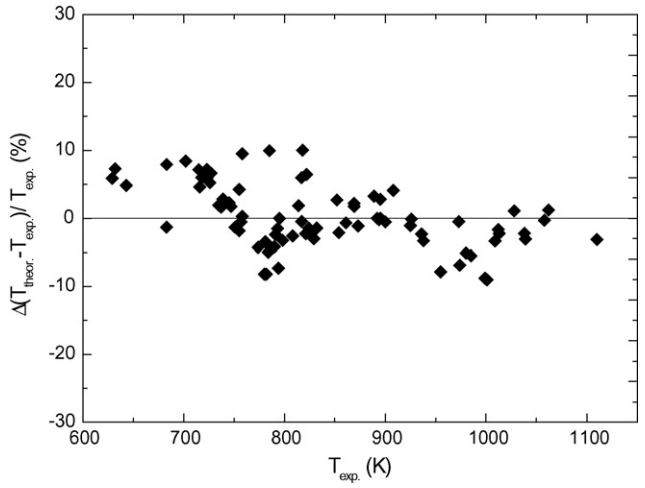

Fig. 6. The difference between the calculated and the experimental ternary liquidus temperature T_{exp} of LiF–BeF_2–ZrF_4 system, normalized by T_{exp}, vs. T_{exp}.

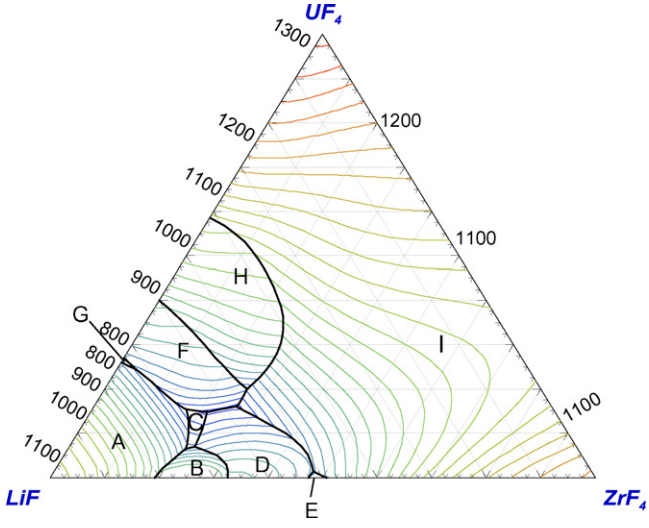

Fig. 7. Liquidus projection of the LiF–ZrF_4–UF_4 ternary system. Primary phase fields: (A) LiF; (B) Li_3ZrF_7; (C) Li_4ZrF_8; (D) Li_2ZrF_6; (E) $Li_3Zr_4F_{19}$; (F) $LiUF_5$; (G) Li_4UF_8; (H) LiU_4F_{17}; (I) $(U,Zr)F_4$.

3.3. Nuclear fuel compositions

The main purpose of the thermodynamic investigation of the LiF–BeF_2–ZrF_4–UF_4 system is its possible use as a fuel in a molten salt reactor. For such an application it is necessary to have a melting point well below the operating temperature to reduce the risk of sudden "freezing" at certain circumstances. The aim of this work was to find the optimum composition and melting temperature of the fuel. In Ref. [10] the typical entering temperature of the fuel into the reactor was mentioned to be 838 K (565 °C). A safety margin of 67 K (the same margin as in Molten Salt Breeder Reactor Design) was kept in our work and the temperature of 771 K was taken as reference point to predict whether the eutectic temperature and composition are suited for the molten salt fuel.

It was observed that the quaternary eutectic of the system is at $T = 651$ K and $X_{LiF} = 0.579$, $X_{BeF_2} = 0.059$, $X_{ZrF_4} = 0.234$, $X_{UF_4} = 0.128$. It is low enough to fulfill our temperature criteria, but the concentration of UF_4 and ZrF_4 are very high and must be

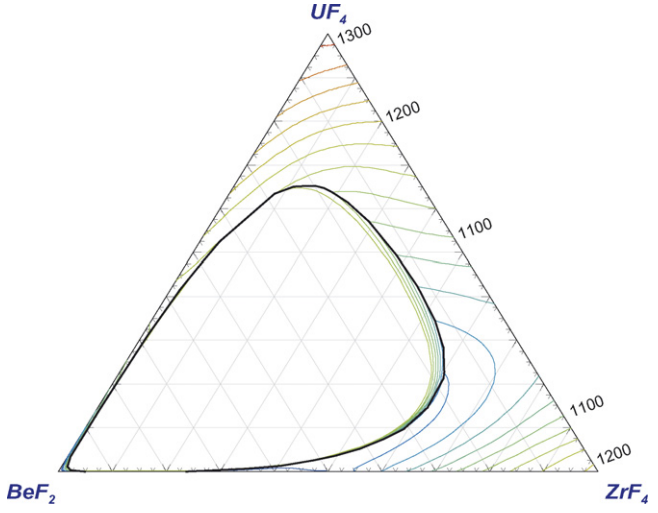

Fig. 8. Liquidus projection of the BeF_2–ZrF_4–UF_4 ternary system. $(U,Zr)F_4$ solid solution is the primary phase in whole the region of the diagram.

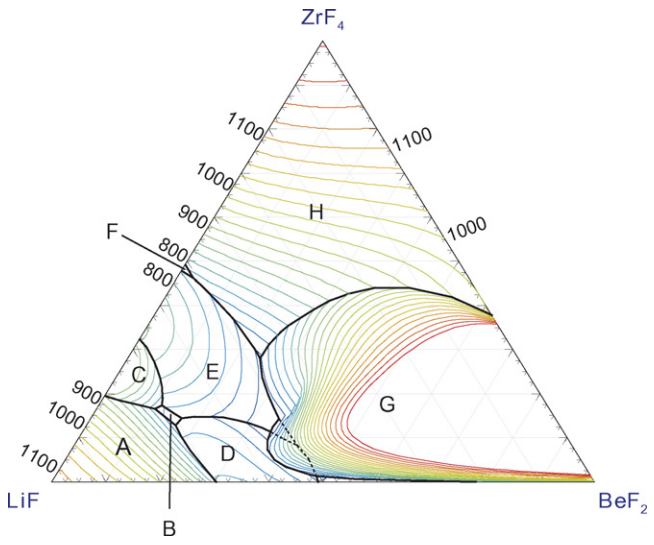

Fig. 9. Liquidus projection of the LiF–BeF_2–ZrF_4–UF_4 system with constant amount of UF_4 equal to 0.83 mol%, the dashed line represents the liquidus line in equilibrium with two immiscible liquid phases. Primary phase fields: (A) LiF; (B) Li_4ZrF_8; (C) Li_3ZrF_7; (D) Li_2BeF_4; (E) Li_2ZrF_6; (F) $Li_3Zr_4F_{19}$; (G) $BeF_2(\beta)$; (H) ZrF_4.

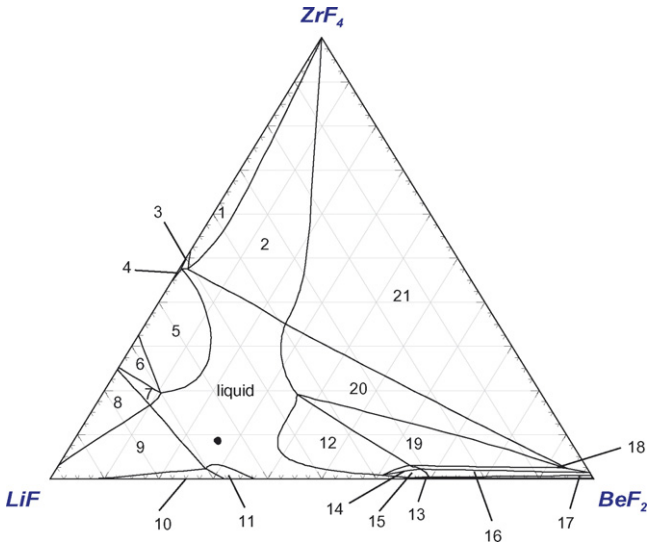

Fig. 10. Isothermal section of the phase diagram at $X_{UF_4} = 0.0083$ and $T = 750$ K. The dot in liquid field represents the recommended fuel composition. Phase fields: (1) $(U,Zr)F_4 + Li_3Zr_4F_{19} + L$; (2) $(U,Zr)F_4 + L$; (3) $Li_3Zr_4F_{19} + L$; (4) $Li_2ZrF_6 + Li_3Zr_4F_{19} + L$; (5) $Li_2ZrF_6 + L$; (6) $Li_3ZrF_7 + Li_2ZrF_6 + L$; (7) $Li_3ZrF_7 + L$; (8) $Li_3ZrF_7 + LiF + L$; (9) $LiF + L$; (10) $Li_2BeF_4 + LiF + L$; (11) $Li_2BeF_4 + L$; (12) $L_1 + L_2$; (13) $LiU_4F_{17} + L$; (14) $(U,Zr)F_4 + L_1 + L_2$; (15) $(U,Zr)F_4 + L$; (16) $(U,Zr)F_4 + L + BeF_2(\beta)$; (17) $(U,Zr)F_4 + BeF_2(\beta) + LiU_4F_{17} + L$; (18) $(U,Zr)F_4 + BeF_2(\beta) + L_1 + L_2$; (19) $BeF_2(\beta) + L_1 + L_2$; (20) $BeF_2(\beta) + L$; (21) $(U,Zr)F_4 + BeF_2(\beta) + L$; L: liquid.

decreased. It is worthwhile to say that according to the ORNL concepts from 1960s, the concentration of UF_4 should be around 1 mol% depending on the exact concept of the reactor, especially on the frequency of the clean up treatment. Concerning the other three compounds there is more flexibility when optimizing the composition, but we should keep in mind that the more ZrF_4 is added the higher the vapor pressure and the more BeF_2 is present the higher the viscosity.

Since the most strict criteria when considering the concentrations are for the UF_4 compound, we plotted a pseudo-ternary phase diagram with the fixed amount of this compound set to $X_{UF_4} = 0.0083$. This value corresponds to the MSRE concept. The phase diagram is shown in Fig. 9, where the lowest melting temperature that is in equilibrium with homogeneous liquid phase corresponds to $T = 675$ K and $X_{LiF} = 0.505$, $X_{BeF_2} = 0.346$, $X_{ZrF_4} = 0.141$, $X_{UF_4} = 0.0083$ (it is indeed true that the lowest eutectic of this system is at $T = 669$ K and is represented by the dashed line in Fig. 9, but this point is in equilibrium with two liquid phases and is not considered). This temperature and composition seem to be very promising for the molten salt fuel, but this point is very close to the miscibility gap and that could cause trouble when a slight composition shift towards the BeF_2 corner occurs. Nevertheless the temperature margin is wide enough to change the composition to a more stable field. Fig. 10 shows the isothermal phase diagram ($T = 771$ K, our reference temperature) with the wide liquid field and the point of a possible fuel composition for this system.

The recommended fuel composition in Fig. 10 corresponds to $X_{LiF} = 0.644$, $X_{BeF_2} = 0.265$, $X_{ZrF_4} = 0.083$, $X_{UF_4} = 0.0083$. The concentration of ZrF_4 here is slightly higher than the one proposed in MSRE (~5%), therefore the vapor pressure for the temperatures 800 K and 1100 K was calculated. The inlet and outlet temperatures in nuclear reactor will be most likely within this range. For 800 K the vapor pressure is 9.31×10^{-8} bar, while for 1100 K, the vapor pressure is 4.13×10^{-4} bar, thus fulfilling the criteria for molten salt reactor assembly.

References

[1] W.R. Grimes, Nucl. Appl. Tech. 8 (1969) 137.
[2] A.D. Pelton, CALPHAD 25 (2001) 319.
[3] C.W. Bale, P. Chartrand, S.A. Degterov, G. Eriksson, K. Hack, R. Ben-Mahfoud, J. Melançon, A.D. Pelton, S. Petersen, CALPHAD 62 (2002) 189.
[4] M. Pelikan, D.E. Goldberg, E. Cantú-Paz, in: W. Banzhaf, J. Daida, A.E. Eiben, M.H. Garzon, V. Honavar, M. Jakiela, R.E. Smith (Eds.), Proceedings of the Genetic and Evolutionary Computation Conference GECCO-99, vol. I, Morgan Kaufmann Publishers, San Fransisco, CA, 1999, pp. 525–532, http://citeseer.ist.psu.edu/pelikan99boa.html.
[5] R.J.M. Konings, J.P.M. van der Meer, E. Walle, Chemical aspects of molten salt reactor fuel, Tech. Rep., iTU-TN 2005/25, 2005.
[6] J.P.M. van der Meer, R.J.M. Konings, K. Hack, H.A.J. Oonk, Chem. Mater. 18 (2006) 510–517.
[7] R.E. Thoma, H. Insley, H.A. Friedman, G.M. Hebert, J. Chem. Eng. Data 10 (1965) 219.
[8] R.E. Thoma, H. Insley, H.A. Friedman, G.M. Hebert, J. Nucl. Mater. 27 (1968) 166.
[9] C.J. Barton, W.R. Grimes, H. Insley, R.E. Moore, R. Thoma, J. Phys. Chem. 62 (1958) 665.
[10] C. Forsberg, Proceedings of the Americas Nuclear Energy Symposium American Nuclear Society (ANES 2002), Miami, Florida, 2002.